

Studying the Strangeness D -Term in Hall C via Exclusive ϕ Electroproduction

A Letter of Intent to Jefferson Lab PAC 52

W. Armstrong, S. Joosten^{*}, H.T. Klest^{*†}, S. Lee, Z.-E. Meziani, C. Peng, S. Prasad, P. Reimer,
M. Žurek

Physics Division, Argonne National Laboratory, Lemont, IL, USA

G. Niculescu, I. Niculescu

James Madison University, Harrisonburg, VA, USA

H. Atac, N. Ifat, S. Shrestha, N. Sparveris

Temple University, Philadelphia, PA, USA

H. Szumila-Vance^{*}

Florida International University, Miami, FL, USA

W. Li

Mississippi State University, Starkville, MS, USA

^{*}Spokesperson
[†]Contact person

Executive Summary

Main Physics Goals:

We propose a measurement of exclusive electroproduction of ϕ mesons near threshold in Hall C. We will measure the $|t|$ -dependence of the exclusive ϕ cross section, $d\sigma/d|t|$, which has recently been proposed as an observable sensitive to the strangeness D -term [1]. The contribution of u and d quarks to the mechanical structure of the proton was recently extracted from DVCS data [2–4]. The contribution of strangeness to the total quark D -term is presently unknown, with different arguments favoring D_s being large, small, or even having opposite sign from the total quark D -term. In addition, this dataset will allow us to perform measurements of other exclusive meson final states, including the first measurement of η' electroproduction.

Proposed Measurement:

We request 30 days of beam to measure the cross section for near-threshold deep exclusive ϕ production as a function of momentum transfer $|t|$ via the missing mass of the $H(e, e'p)$ reaction using the spectrometers in Hall C. We will use the SHMS at 13° to detect electrons with a central momentum of 6.7 GeV and the HMS at 32° to detect protons with central momenta of 1.1 GeV and 1.8 GeV. The electron kinematics correspond to an average Q^2 of 3.4 GeV² and an average W of 2.2 GeV. The observable sensitive to the strangeness D -term is the shape of the $|t|$ -distribution, particularly at low- $|t|$, where a non-zero D_s manifests as a softening or even an inversion of the $|t|$ -slope. We plan to measure for 16.5 days with the HMS set to detect protons at 1.1 GeV to measure close to $t_{min.}$. We also propose to measure for 11.5 days at higher $|t|$ to pin down the normalization of the cross section as well as to provide a larger lever arm for extracting the functional form of the $|t|$ -distribution.

Specific Requirements on Detectors, Targets, and Beam:

This measurement will use the standard Hall C equipment. We propose to utilize the 10 cm liquid hydrogen target with an unpolarized electron beam at an energy of 10.6 GeV and a beam current of 75 μ A.

1 Introduction

The past seven decades have seen tremendous advancement in the understanding of the electromagnetic structure of the proton, in particular via the measurement of the electromagnetic form factors. These form factors are defined through the matrix elements of the electromagnetic current operator and encapsulate the non-pointlike nature of the nucleon charge distribution. More recently, enabled by substantial progress in theoretical understanding and experimental precision, the first headway has been made into understanding the *gravitational* structure of the proton. Our proposed measurement seeks to extend this research program beyond the valence quarks into the strangeness sector.

Analogous to the electromagnetic case, the proton gravitational form factors (GFFs) encode information about the matrix elements of the energy-momentum tensor. They are often written as:

$$\begin{aligned} \langle p', \vec{s}' | T_a^{\mu\nu} | p, \vec{s} \rangle = \bar{u}(p', \vec{s}') \left[A_a(t) \frac{P^\mu P^\nu}{m_N} + D_a(t) \frac{\Delta^\mu \Delta^\nu - g^{\mu\nu} \Delta^2}{4m_N} + \bar{C}_a(t) m_N g^{\mu\nu} \right. \\ \left. + J_a(t) \frac{P^{\{\mu} i \sigma^{\nu\} \lambda} \Delta_\lambda}{m_N} - S_a(t) \frac{P^{[\mu} i \sigma^{\nu] \lambda} \Delta_\lambda}{m_N} \right] u(p, \vec{s}), \end{aligned} \quad (1)$$

where $T^{\hat{\mu}\nu}$ is the energy-momentum tensor of QCD, $a^{\{\mu} b^{\nu\}} = (a^\mu b^\nu + a^\nu b^\mu)/2$, $u(p, s)$ is the Dirac spinor, $P = (p + p')/2$, $|p, \vec{s}\rangle$ is a proton with spin eigenstate s and four-momentum p , m_N is the mass of the nucleon, $\Delta = p' - p$, and $t = \Delta^2$ [5]. The functions $A_a(t)$, $D_a(t)$, $\bar{C}_a(t)$, $J_a(t)$, and $S_a(t)$ are the GFFs. The subscript a denotes the parton flavor, i.e., $D_s(t)$ represents the strangeness D -term.

The GFFs at zero momentum transfer represent fundamental properties of the proton. These properties, including mass, spin, and the D -term, describe how the proton reacts to changes in the space-time metric [6]. Strong constraints are placed on these properties and their corresponding gravitational form factors by symmetries and existing experimental measurements, with the D -term as the notable exception. The D -term encodes the spatial distributions of shear forces and pressure in the proton. Its forward limit, $D(t=0)$, is the least well-known fundamental property of the proton [6]. The total D -term, $D(t=0)$, can be broken down into its partonic components via a sum rule,

$$D(0) = D_g(0) + D_q(0) = D_g(0) + D_u(0) + D_d(0) + D_s(0) + \dots$$

Recently, DVCS data has been used to extract the combined $u+d$ quark D -term [3], and near-threshold exclusive J/ψ photoproduction has been used to determine the gluonic D -term [7]. The results on the $u+d$ quark D -term provided the first measurement of the mechanical radius [2] and radial pressure distribution [3] of the proton¹, under the assumption that $D_s = 0$.

One may expect that due to the relatively small fraction of strangeness in the valence region of the proton, $D_s(0)$ should be negligible. However, an argument derived in the large N_c limit [1, 9] suggests that the D -term should be approximately flavor-independent, i.e. $D_u \approx D_d$, in spite of the very different contributions to the proton spin and momentum of the up and down quarks. The existing lattice data seem to confirm this D -term flavor-independence prediction [10]; the up quark provides approximately 70% of the total quark contribution to the A form factor and nearly 100% to the J form factor, yet up and down quarks contribute approximately equally to the D -term. Extending the large N_c argument to include also the third light quark species, $D_s(0)$ may still be sizable despite the small strange quark contribution to the momentum and spin structure of the proton in the valence region. Another hint towards a non-negligible value of $D_s(0)$ was provided in Refs. [11, 12]. The authors applied the chiral quark-soliton model and found that $D_s(0) \approx 0.5D_u \approx 0.5D_d$, indicating that strangeness may play a substantial role in the mechanical structure of the proton.

Motivated by these arguments, we propose to measure $d\sigma/d|t|$ in deep exclusive ϕ meson production with the goal of studying the last remaining light quark component of the total D -term, thereby observing for the first time the contribution of a non-valence quark to the mechanical properties of the proton.

2 Theory and Kinematics

Recently, the authors of Ref. [1] suggested that exclusive electroproduction of ϕ mesons near threshold can provide the first window into the contribution of strangeness to the total D -term. This is at present

¹See, however, the discussion in Ref. [8].

the only proposed observable sensitive to the strangeness D -term. An example diagram of this process is shown in Fig. 1. “Near threshold” refers to the kinematic region in which $W \approx m_N + m_\phi$, where W is the hadronic center-of-mass energy, defined as $W^2 = m_N^2 + 2m_N(E - E') - Q^2$, with E and E' referring to the energies of the beam and scattered electron, respectively.

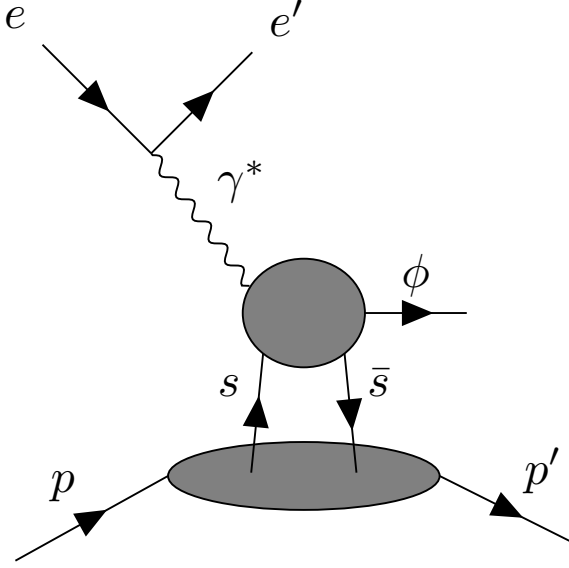


Figure 1: Example diagram contributing to deep exclusive ϕ production. This process is sensitive to the strangeness D -term.

A majority of the existing experimental measurements of exclusive ϕ production were performed in photoproduction [13, 14], i.e., $Q^2 \approx 0 \text{ GeV}^2$. Studying the electroproduction of ϕ at high Q^2 enables the clean theoretical interpretation of results in the near-threshold region via the operator product expansion (OPE), as will be shown in this section. A typical challenge in performing calculations of meson production near threshold is that as Q^2 becomes large, the kinematics shift away from the forward limit ($t \approx 0 \text{ GeV}^2$), where the standard VMD and two-gluon form factor techniques are applicable. A feature of near-threshold reactions is that t , defined as $t = \Delta^2 = (p' - p)^2$, is typically not small. In fact, for production at threshold

$$|t_{thr.}| = \frac{m_N(m_V^2 + Q^2)}{m_N + m_V}. \quad (2)$$

As an example, for production of ϕ at threshold with Q^2 of 3.4 GeV^2 , $|t_{thr.}| = 2.1 \text{ GeV}^2$, which is reasonably far from the forward limit. To handle this, the authors of Refs. [1, 15] devised a method to calculate the relevant non-forward matrix elements using the OPE.

We recount the necessary features of the calculation here. The ϕ production cross section can be written as:

$$\frac{d\sigma}{dWdQ^2} = \frac{\alpha_{em}^2}{4\pi} \frac{1}{16(P \cdot \ell)^2 Q^4 P_{cm}} \int \frac{d\phi_\ell}{2\pi} L_{\mu\nu} \int dt \frac{1}{2} \sum_{spin} \langle P | J_{em}^\mu(-q) | P' \phi \rangle \langle P' \phi | J_{em}^\nu(q) | P \rangle, \quad (3)$$

where J_{em} is the electromagnetic current and P_{cm} is the proton momentum in the $\gamma^* p$ center-of-mass frame. The OPE permits calculation of the off-forward matrix element $\langle P' \phi | J_{em}^\nu(q) | P \rangle$, as described in detail in Ref. [15].

To provide numerical results for $d\sigma/d|t|$, the matrix elements calculated above and the following parameterization of the GFFs are utilized:

$$\langle P' | T_s^{\alpha\beta} | P \rangle = \bar{u}(P') \left[A_s(t) \gamma^{(\alpha} \bar{P}^{\beta)} + B_s(t) \frac{\bar{P}^{(\alpha} i \sigma^{\beta)\lambda} \Delta_\lambda}{2m_N} + D_s(t) \frac{\Delta^\alpha \Delta^\beta - g^{\alpha\beta} \Delta^2}{4m_N} + \bar{C}_s(t) m_N g^{\alpha\beta} \right] u(P), \quad (4)$$

where $\bar{P} = \frac{P+P'}{2}$, $\Delta^\mu = P'^\mu - P^\mu$, and $t = \Delta^2$. To produce numerical predictions that can be compared to the data, external information must be used to constrain some of these parameters. The authors

use the assumption $\bar{C}_s = -\frac{1}{4}A_s$, i.e., that the trace anomaly is insignificant in the strangeness sector², and that B_s is negligible, motivated by the finding that B_{u+d} is small [16]. With these form factors externally constrained, the remaining form factors that contribute to the ϕ production cross section are A_s and D_s . The standard dipole and tripole forms are employed to capture the $|t|$ -dependence of the form factors $A_s(t)$ and $D_s(t)$, respectively³:

$$A_s(t) = \frac{A_s(0)}{(1 - t/m_A^2)^2}, \quad D_s(t) = \frac{D_s(0)}{(1 - t/m_D^2)^3}, \quad (5)$$

where $A_s(0)$, m_A , and m_D are taken to be 0.025, 1.17 GeV, and 0.83 GeV, respectively, as suggested by the most recent lattice results [10]. Note that with the experimental data we propose to collect, these parameters could also be extracted directly from a combined fit instead of entirely relying on the lattice results as we do here. Assuming the above values of $A_s(0)$, m_A , and m_D , the predicted cross sections as a function of $|t|$ for various values of $D_s(0)$ are shown in Fig. 2. The softening of the $|t|$

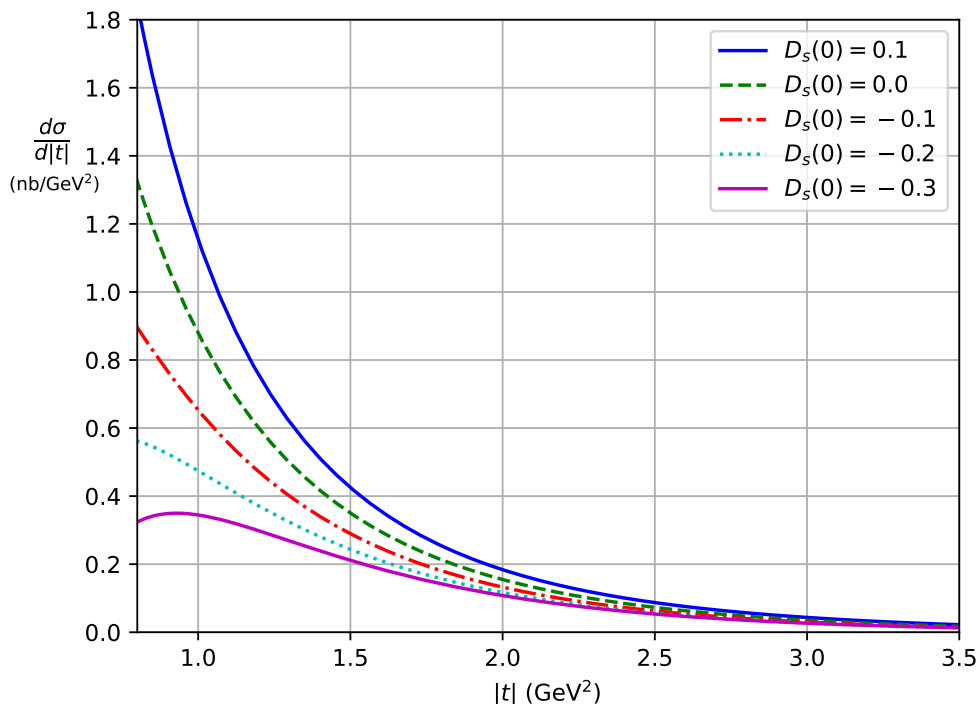


Figure 2: Theoretical predictions for $d\sigma/d|t|$ at $Q^2 = 3.4 \text{ GeV}^2$ and $W = 2.2 \text{ GeV}$ with different assumptions for $D_s(0)$. In this kinematic range $t_{\min} \approx 0.7 \text{ GeV}^2$. It can be seen that the introduction of a non-zero $D_s(0)$ has a large impact on the shape and size of the cross section.

slope is a result of the factor of Δ multiplying D_s in Eq. 4. For larger values of $D_s(0)$, the cross section $d\sigma/d|t|$ receives a larger contribution from the D -term compared to the A -term and thus experiences more of a suppression at low- $|t|$. A naive physical interpretation of the effect of the D -term on the cross section is that an $s\bar{s}$ pair is less likely to stay bound as a ϕ meson if the strange quark pressure is large and pointing outward, i.e., if $D_s(0)$ is negative and large. On the contrary, if $D_s(0)$ is positive, the ϕ cross section will be enhanced by the confining pressure of the strange quarks in the proton tending to bind the $s\bar{s}$ pair into a ϕ .

The overall normalization of the prediction is at present poorly constrained by the theory alone due to non-negligible twist-two higher spin effects which have not yet been calculated. In the model curves shown in Fig. 2, the magnitude of the cross section was determined by comparison with the

² \bar{C} is additionally constrained by the requirement that $\bar{C}_q + \bar{C}_g = 0$.

³These functional forms are motivated by the asymptotics of perturbative calculations performed at large- $|t|$ [17, 18].

existing ϕ electroproduction data from CLAS [19] under the assumption that $D_s(0) = 0$. This normalization additionally agrees well with the parameterization used in the CLAS12 proposal [20], which we reproduce in the Appendix 8.

The separated u, d , and s quark contributions to the D -term were determined on the lattice in Ref. [10]. In this work, the value of $D_s(0)$ is found to be small, with $D_s(0) = -0.18 \pm 0.17$ and $D_s(0) = -0.08 \pm 0.17$, for dipole and z -expansion fits, respectively. These values are consistent with zero, although the relative uncertainties are large and the extraction has not yet been performed in the continuum limit. It is also worth mentioning that the current lattice results do not conclusively preclude the possibility that $D_s(0)$ is positive. In this intriguing scenario, the strange quarks would contribute a pressure in the opposite direction from the valence quarks as extracted from DVCS, suggesting a fundamental difference between the mechanical properties of valence and sea quarks.

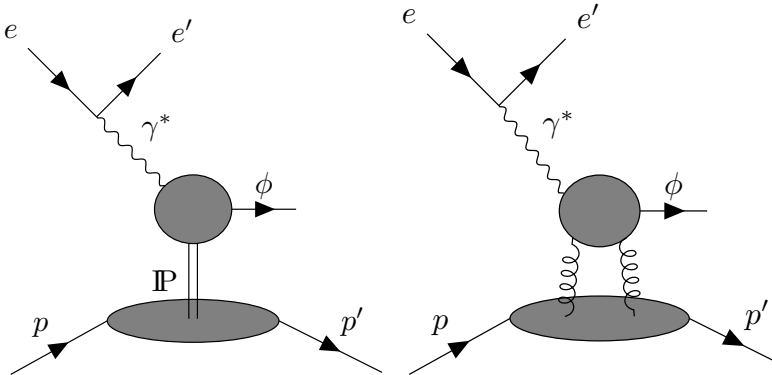


Figure 3: Additional processes that can contribute to exclusive ϕ electroproduction. Left: Example diagram for exclusive ϕ electroproduction via pomeron exchange. Right: Example diagram for exclusive ϕ electroproduction via two gluon exchange.

So far, we have not discussed the other processes that can contribute to exclusive ϕ electroproduction. The authors of Ref. [21] investigated pomeron and meson exchange, shown in the left panel of Fig. 3, as a model of ϕ electroproduction. The authors find reasonable agreement with the existing data on the Q^2 dependence of the longitudinal and transverse cross sections, which are dominated by scalar meson and pomeron exchange, respectively. The model additionally reproduces the $|t|$ -dependence of the data at $Q^2 < 1 \text{ GeV}^2$ and $\langle W \rangle = 2.9 \text{ GeV}$ but has difficulty describing the higher Q^2 and lower W CLAS data at $\langle Q^2 \rangle = 2.2 \text{ GeV}^2$ and $\langle W \rangle = 2.5 \text{ GeV}$, suggesting that the hadronic picture breaks down at higher Q^2 .

The two gluon exchange process, sketched in the right panel of Fig. 3, has been shown by various studies [22–25] to dominate in exclusive ϕ production by longitudinally polarized virtual photons away from threshold, particularly at low- x , thereby providing access to the gluon GPD. Close to the threshold, the GPD picture formally breaks down due to the low relative momenta of the outgoing meson and baryon [1, 26]. For these low relative momentum configurations, there is no suppression of final-state interactions, which is crucial for factorization [26]. In spite of this, the GPD model based on the double distribution approach provides reasonable agreement with data on ϕ production by longitudinally polarized virtual photons integrated over the region $2.1 < W < 2.9 \text{ GeV}$ from CLAS [19, 27]. Furthermore, the authors of Ref. [28] analyzed the longitudinal ϕ production cross section in a holographic approach and found reasonable agreement between the existing ϕ electroproduction data and their calculation utilizing only the evolved gluon GPD.

The calculation of Ref. [1] calculates $d\sigma/d|t|$ purely for the coupling to strange quarks as sketched in Fig. 1. Ref. [1] provides an argument indicating that the strange quarks, via the process shown in Fig. 1, contribute more than the gluons in the near-threshold region for *unpolarized* virtual photons. The photon polarization is a key point of distinction between the GPD and OPE approaches; in the OPE approach, the *transverse* component of the virtual photon dominates. While an L/T separated cross section is presently beyond the scope of this LOI, the CLAS12 proposal [20] will provide L/T separated cross sections in similar kinematics, which will help to clarify the situation substantially. In the OPE approach, the effect of the gluon GFFs is suppressed by a factor $\alpha_s/4\pi$. Furthermore, twist-two, higher spin operators, which are small in the gluon case but significant in the s -quark case, provide

an additional boost to the coupling to strangeness. These two factors suggest that the contribution from gluons is around a factor of two smaller than from strange quarks.

To summarize, the GPD approach is valid in the region away from threshold and for longitudinally polarized photons, the pomeron/meson exchange approach appears to be valid in the region of $Q^2 < 1$ GeV, and the OPE approach is valid in the near-threshold region and is dominated by transversely polarized photons. Unavoidably both the gluon and strange quark processes contribute to ϕ production. Better understanding the interplay of the strange and gluon GFFs, and how they affect $d\sigma/d|t|$, will be one of our goals for the full proposal. The approach of Ref. [1] was originally employed to calculate the effect of D_g on the J/ψ electroproduction cross section [15], so there exists at least one feasible pathway towards a self-consistent theoretical description of both the gluon and strange quark contributions to the ϕ $d\sigma/d|t|$. Given that exclusive ϕ is at present the only proposed experimental observable sensitive to the strangeness D -term, it is evident that further theoretical study and additional data on this topic are crucial to completely understand the D -term in terms of its partonic constituents. For now, we provide our experimental projections for $d\sigma/d|t|$ and estimate our sensitivity to $D_s(0)$ following the assumptions of Ref. [1], with the understanding that the addition of other processes will dilute the sensitivity.

3 Experimental Technique

The only existing measurements of ϕ electroproduction in the region of $W < 3$ GeV were performed by CLAS [19, 29] at beam energies of 4.2 and 5.8 GeV. The authors of Ref. [1] were unable to compare their model directly to the existing CLAS data due to the large bins in Q^2 and W employed in those measurements. Since the shape of the $|t|$ -distribution near threshold is sensitive to W and Q^2 , an extraction of $D_s(0)$ via the $|t|$ -distribution should seek to minimize the bin size in Q^2 and W as much as possible. For the same reason, it is important that the data be binned in $|t|$ rather than $|t - t_{\min.}|$. The sharp drop in the cross section in the near-threshold region presents an additional experimental challenge. The Hall C spectrometers, with their narrow angular and momentum acceptance but high luminosity capability, are therefore a natural choice for such a measurement.

The high precision of the Hall C spectrometers allows for measurements of cross sections via the missing mass technique. We propose to leverage this capability to reconstruct the ϕ meson in the missing mass distribution. The missing mass (M_X) is reconstructed as the mass of the four-vector defined by $(\vec{P}_e + \vec{P}_p) - (\vec{P}_{e'} + \vec{P}_{p'})$. This technique has some advantages over reconstructing the full final state. The first is that all decay modes of the ϕ contribute, i.e., there is no reduction in the measured event yield due to the branching fraction. Another advantage is the fact that identifying the scattered electron and proton is typically easier than identifying kaons from the ϕ decay, which are easily confused for the much more copiously produced pions and protons. The primary disadvantage of the missing mass technique is that other processes inevitably will produce similar $e'p'$ missing masses to the exclusive ϕ events. This results in a large and partially irreducible background that must be subtracted to recover the true ϕ cross section. We describe the background in detail in Section 3.1.

To reach low values of $|t|$, the HMS will be used to detect the proton, while the electron will be detected in the SHMS. Since our goal is to fit the $|t|$ -distribution to study $D_s(0)$, we propose two spectrometer settings. The primary setting will sit at low values of $|t|$ where the $|t|$ -distribution is most sensitive to the value of $D_s(0)$. The secondary setting will sit at higher values of $|t|$ to determine the absolute normalization of the cross section and provide additional lever arm to constrain the fit.

To simulate the exclusive ϕ channel, we interfaced the cross section parameterization developed for the CLAS12 exclusive ϕ proposal [20] to the lAger event generator [30]. The parameterization successfully reproduces the existing world data on σ_T , σ_L , and R [19, 29, 31–34]. For the $|t|$ dependence, we assume a dipole form. A more complete description of this parameterization is provided in the appendix of this LOI [8].

To evaluate the acceptance and resolution of the Hall C spectrometers, we utilized the standard Hall C fast Monte Carlo program, SIMC [35]. Our proposed settings were initially determined by maximizing the event statistics for exclusive ϕ in the relevant region of $|t|$ while keeping Q^2 reasonably high and W near the threshold value of 1.96 GeV. In addition, the settings were further optimized to reduce the random coincidence and physics event backgrounds as much as possible.

In the HMS, the time-of-flight for particles with 1.8 GeV of momentum is 94, 86, and 83 ns for protons, kaons, and pions, respectively. Given the HMS time-of-flight resolution of less than 200 ps,

Setting	$P_{e'}$ SHMS	$\theta_{e'}$ SHMS	$P_{p'}$ HMS	$\theta_{p'}$ HMS	Beam Current (μA)
Low $ t $	6.7 GeV	13°	1.1 GeV	32°	75
High $ t $	6.7 GeV	13°	1.8 GeV	32°	75

Table 1: Proposed spectrometer settings and beam currents. The SHMS setting corresponds to $Q^2 \approx 3.4 \text{ GeV}^2$ and $W \approx 2.2 \text{ GeV}$ for exclusive ϕ events.

we expect no difficulty in identifying the protons with time-of-flight alone.

The HMS has been used successfully in similar settings with relatively low proton momenta by the E12-15-001 VCS experiment. The proton absorption was estimated for that experiment to be around $5 \pm 0.5\%$ for protons of momenta 0.8 to 0.9 GeV [36]. Furthermore, the $N\Delta$ proposal to PAC 50 [37] demonstrated the feasibility of detecting protons with momenta of around 0.4 GeV, so we foresee no technical issues with our proton momentum settings of 1.1 and 1.8 GeV.

3.1 Backgrounds

The two primary physics backgrounds are exclusive production of non- ϕ mesons and continuum processes, including multi-pion production and DIS. These physics processes will unavoidably produce a background in the missing mass distribution upon which the ϕ peak will sit, and understanding this background is a vital component of this experiment. The masses and widths are reproduced in Table 2.

Meson	Mass (MeV)	Width (MeV)
Vector Mesons		
ρ	775.3	149.1
ω	782.7	8.68
ϕ	1019.46	4.25
Pseudoscalar Mesons		
π	134.98	small
K	493.68	small
η	547.86	0.00131
η'	957.78	0.196

Table 2: Masses and widths of vector and pseudoscalar mesons (in MeV) relevant for this measurement.

The general-purpose MC generators PYTHIA6 (PYTHIA eRHIC tune) and LEPTO (CLASDIS tune) were used to evaluate the contributions to the background from exclusive production of mesons other than the ϕ , as well as DIS and other continuum processes. The cross section of the continuum background was nearly identical between the two programs in the region underneath the ϕ peak, although LEPTO predicts a larger cross section at higher values of M_X , and PYTHIA6 predicts a larger cross section at lower values of M_X . The predicted M_X distributions from LEPTO and PYTHIA6 in the region $2.5 < Q^2 < 6 \text{ GeV}^2$ are shown in Fig. 4. The cross section for η' has not been measured in the kinematic region of interest for this study, and its proximity to the ϕ , only 62 MeV away, makes it an important background to understand. Both PYTHIA6 and LEPTO predict that in the kinematic region $2.5 < Q^2 < 6 \text{ GeV}^2$, the η' cross section is larger than that of the ϕ . The η' was previously observed to be larger than the ϕ during the 6 GeV u -channel $\omega H(e, e'p)$ analysis of Refs. [38, 39]. However, Ref. [40] computes the η' cross section using a GPD model for $Q^2 = 3.44 \text{ GeV}^2$ and $W = 3.83 \text{ GeV}$ and finds that it is of similar size as our estimate for the ϕ . PYTHIA6 predicts a very large η' cross section, almost a factor of 20 larger than ϕ in this phase space, while the η' cross section in LEPTO is around a factor of four smaller. The existing photoproduction data suggest that at $W \approx 2.2 \text{ GeV}$, the ratio $\sigma_{\eta'}/\sigma_{\phi}$ is around 2, a feature that PYTHIA6 correctly reproduces. PYTHIA6 additionally agrees within a factor of two with the ϕ electroproduction cross section derived from the combination of lAger and the CLAS12 proposal parameterization. Therefore, we employ

PYTHIA6 to provide an estimate for the background under the ϕ peak, with the understanding that it likely provides a "worst-case" estimate of the background from η' .

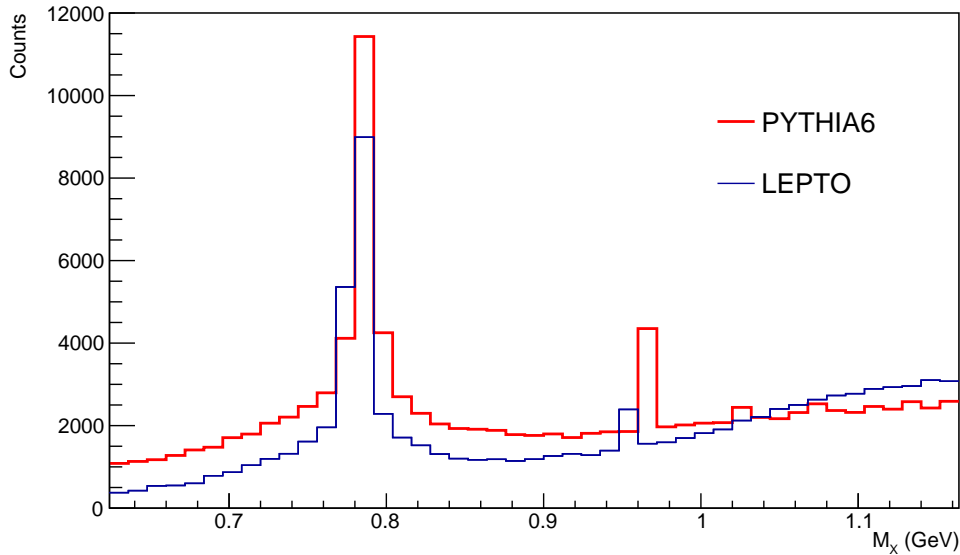


Figure 4: Predicted missing mass distributions from PYTHIA6 and LEPTO. The two distributions are generated with the same integrated luminosity. In the region of the ϕ , the two generators predict very similar event rates.

The η' has a small natural width, but the smearing due to the response of the spectrometers and QED radiation off the electron will cause it to broaden. This effect can be seen in Fig. 5. Using SIMC with detector smearing and external radiation enabled, the missing mass resolution in the region of the ϕ and η' was around 15 MeV for the proposed kinematic settings.

PYTHIA eRHIC has an interface to RADGEN [41] to enable radiative predictions. The background predictions shown above did not use the radiative option, but we studied the differences between the radiative and non-radiative predictions to assess the overall impact of QED radiation. The emission of a photon off the electron in the initial- or final-state typically increases the missing mass of an event significantly, thereby changing the background and signal distributions. QED radiation results in a roughly 15% lower yield of ϕ , as well as a few percent higher continuum background arising from exclusive meson or other low- M_X events being shifted to higher M_X . We independently assessed the contribution of radiative ep elastic events to the background using the ESEPP generator [42]. Roughly 60% of the requested integrated luminosity was generated, and after passing the events through SIMC, 64 events were reconstructed. We therefore expect roughly 100 background events from the radiative elastic ep scattering process, which will have a negligible impact on the measurement. The small impact of these events is largely a result of the fact that the range of y in which we measure ($0.57 < y < 0.66$) is minimally sensitive to radiative effects.

Random coincidences of single particles between the HMS and SHMS provide another source of background. The rate of single charged particles entering the spectrometer acceptances was determined using PYTHIA6 with no cuts on any kinematic variables, thereby including photoproduction processes. For the low- $|t|$ setting, the PYTHIA simulation predicts that the rate of random coincidences between a negatively charged particle in the SHMS acceptance and a positively charged particle in the HMS acceptance is around 500 Hz for a trigger coincidence time window of 70 ns. Assuming the trigger is formed by the HMS and SHMS hodoscopes, the rate is well within the capabilities of the DAQ system. The rate of protons in the HMS is around 230 kHz, and the rate of electrons in the SHMS is around 14 kHz. The total singles rates are given in Tab. 3. The electron rate was determined with radiative effects enabled. The central momentum and angle of the HMS were chosen in part to minimize the singles rate. To assess how these events will impact the analysis, we assume a 2 ns coincidence window and correct particle identification on the electron and proton. These assumptions reduce the random coincidence rate to ≈ 6 Hz. This rate should be compared to the physics background event rate of

Missing Mass Distribution

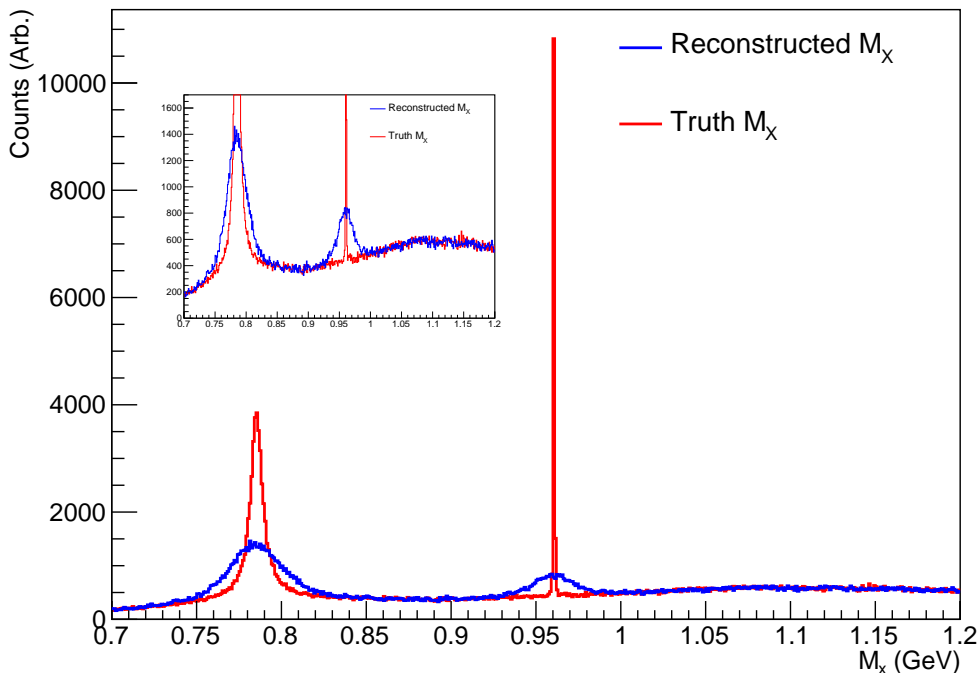


Figure 5: Reconstructed and true missing mass M_X spectra from background events simulated by PYTHIA. The reconstruction is performed by SIMC with external radiation and detector smearing turned on. Exclusive ϕ events have been explicitly removed from this sample. The large and narrow peak in the truth distribution around 0.96 GeV is the η' . The η' is reconstructed with a resolution of around 15 MeV.

≈ 0.2 Hz and the exclusive ϕ event rate of ≈ 0.01 Hz. After analysis cuts, the likelihood that the random coincidence events fall within a missing mass window of ± 100 MeV around the ϕ is 0.15%, compared to 18% for the physics background events. Therefore, the random coincidence background will be $\approx 5\%$ of the total background.

Setting	Total Singles Rate SHMS	e^- Rate SHMS	Total Singles Rate HMS	p^+ Rate HMS
Low $ t $	16 kHz	14 kHz	440 kHz	230 kHz
High $ t $	16 kHz	14 kHz	18 kHz	10 kHz

Table 3: Spectrometer singles rates, determined with PYTHIA6.

3.2 Projected Uncertainty and Required Beam Time

The nature of the prediction of Ref. [1] is such that a measurement of the overall normalization of $d\sigma/d|t|$ is not explicitly necessary for the extraction of $D_s(0)$. We therefore focus mainly on point-to-point uncertainties that can disturb the fit to the theoretical distributions.

Due to the relatively small ϕ cross section, we expect that the extraction of the ϕ signal from the background will prove to be the largest source of uncertainty. For this measurement, higher event statistics will not only increase the signal yield but also reduce the statistical fluctuations in the background that can make signal extraction more challenging. To measure the shape of the $|t|$ slope with reasonable precision, we assume four bins between $0.828 < |t| < 1.078$ GeV² with width of 0.0625 GeV² each for the low- $|t|$ setting. For the high- $|t|$ setting, we assume two bins covering $1.8 < |t| < 2.1$ GeV² and $2.1 < |t| < 2.3$ GeV².

The impact of finite statistical precision on the ϕ signal extraction procedure was evaluated using a replica method. In each replica, the simulated ϕ signal and simulated background data points are jittered in accordance with their statistical uncertainty and the signal extraction is performed. In this case, the signal extraction involves fitting a line to the background in the region of the ϕ , subtracting that line from the measured event yield (signal plus background), and fitting a gaussian to the remainder. Due to the computational challenge of generating a full background dataset, we simulated roughly one day (17 ab^{-1}) of background events and used the shapes of those distributions to parameterize the background in each $|t|$ bin. The parameterization enabled sampling the background distribution with different assumed integrated luminosities and examining the effects on the stability of the signal extraction.

For the extraction of the ϕ yield in the pseudoexperiments, cuts were applied to the reconstructed simulation as they would be in an analysis. The cuts, applied on W , $|t|$, and Q^2 , removed events that kinematically could not have originated from exclusive ϕ production. In the actual experiment, the removed events can be used for a data-driven determination of the background underneath the ϕ peak.

For each $|t|$ bin, 2500 pseudoexperiments were performed, and the standard deviation of the yield extracted from each pseudoexperiment was taken as the combined statistical and signal extraction uncertainty. This procedure results in a point-to-point uncertainty on the ϕ cross section of $\approx 20\%$ for 100 ab^{-1} and $6 - 8\%$ for 297 ab^{-1} in each of our $|t|$ bins. Results from a single pseudoexperiment are shown for the four low- $|t|$ bins in Fig. 6. The mean of the measured yield distribution is often $\approx 15\%$ below the true non-radiative yield due to the radiative tail on the ϕ , which is typically lost in the fitting procedure, and the tendency for the gaussian fit to be narrower than the true signal. Much of this loss of yield could be recovered by unfolding and using a more advanced fit, so we assign a point-to-point uncertainty equal to one quarter of the difference between the true and reconstructed mean yield to account for the combined radiative correction and signal fitting losses in each $|t|$ bin.

Due to the large uncertainty on the cross section and $|t|$ scaling of the η' , we additionally evaluated the impact of scaling the yield of exclusive η' events. The signal extraction procedure was performed with 100%, 50%, and 0% of the PYTHIA6 η' yield present in the M_X distribution. In all cases the extraction performed similarly, with the extraction uncertainty being a few percent higher in the case of the full η' yield predicted by PYTHIA6. If the scaling of the η' cross section as a function of $|t|$ is very different than the ϕ , there could be a bias on the resulting ϕ yield. For our nominal luminosity of 297 ab^{-1} in the low- $|t|$ bins, we anticipate a 4% point-to-point uncertainty on the combined modelling of the η' and continuum background. As is the case with the signal extraction uncertainty, the background modelling uncertainty will grow if the integrated luminosity is decreased.

We would also like to remark that due to the large background underneath the ϕ peak, a total integrated luminosity too far below the requested 297 ab^{-1} (16.5 days at $75 \mu\text{A}$) for the low- $|t|$ setting could endanger the stability of the signal extraction, especially if $D_s(0)$ turns out to be a large negative quantity. For $D_s(0) \approx -0.3$, the exclusive ϕ cross section in the region of our low- $|t|$ setting could be suppressed by a factor of 3 compared to the nominal cross section used in our projections. The choice of 297 ab^{-1} (16.5 days at $75 \mu\text{A}$) for our low- $|t|$ setting provides the headroom to perform a measurement (albeit of degraded precision) even in the case of $D_s(0) = -0.3$ shown in Fig. 2. A more rigorous signal extraction could be performed by taking into account all the information available via a machine learning technique instead of the naive box cut approach applied in this LOI.

At the requested beam current of $75 \mu\text{A}$, the singles rate in the HMS for the low- $|t|$ setting is expected to be high enough to cause a degradation in the tracking efficiency of around 5%. We expect this to enter as a normalization uncertainty between the the two settings individually, since the singles rates vary only between settings. We therefore assign 0.5% as the uncertainty on the low- $|t|$ bins and 2.5% as the uncertainty on the high- $|t|$ bins as a way of quantifying this uncertainty on the fit to the theory curve.

Finally, we assign a flat 3% point-to-point uncertainty on all points, accounting for effects such as pion contamination, bin centering, beam energy, proton absorption, etc., based on the experience of the VCS experiment [36].

3.3 Additional Possible Setups

Our evaluation of the measurement feasibility was performed with the standard two-arm Hall C setup, but we describe in this subsection some possible options that could enhance the quality of the measurement if deemed technically feasible.

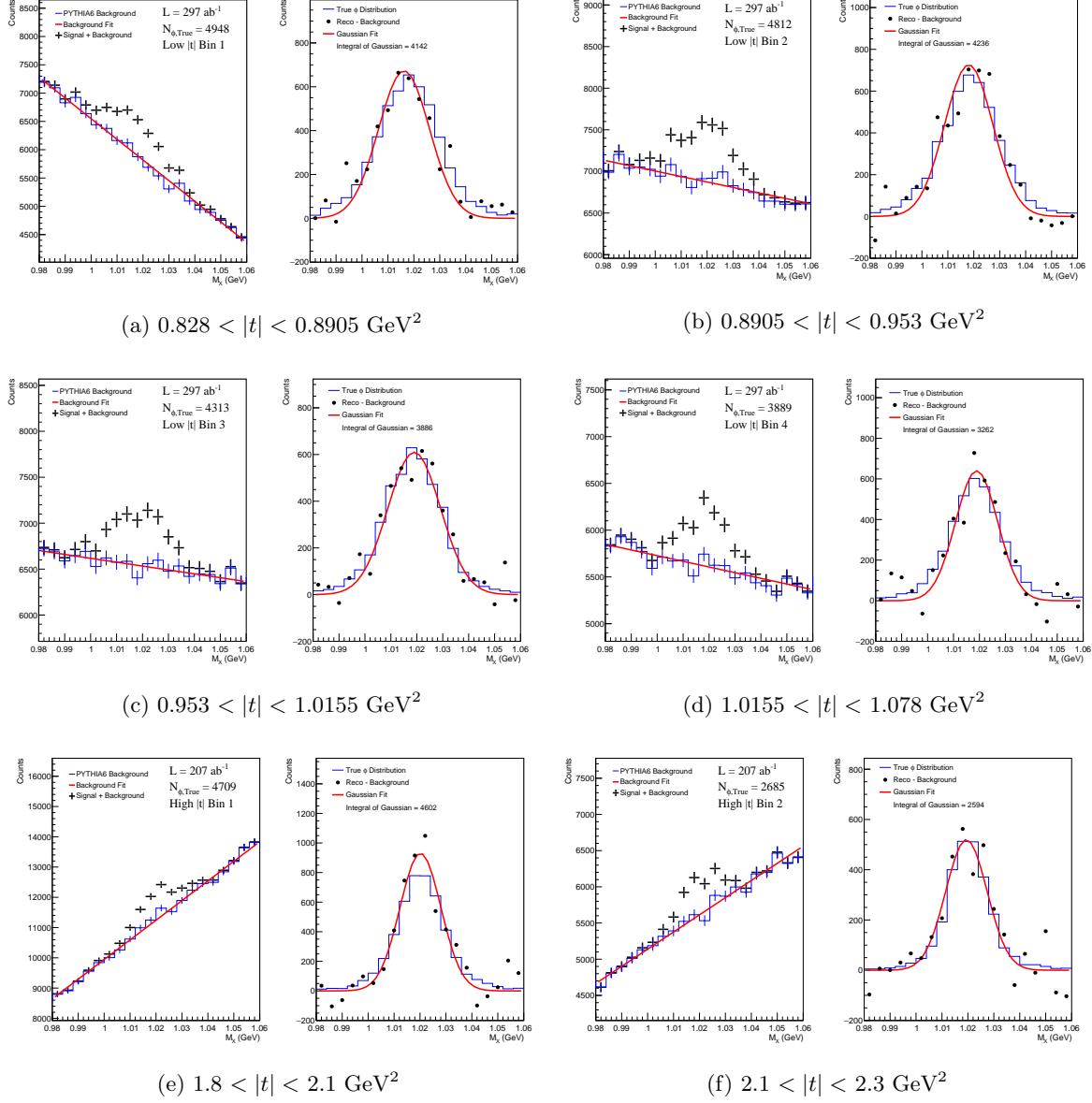


Figure 6: Example results of pseudoexperiments used to estimate the statistical and signal extraction uncertainty. Left panels show the signal and background as it would appear in the experimental data. Right panels show the background subtracted pseudodata (black points) distributions fit with a gaussian function (red curve) and the true generated ϕ distributions (blue histogram).

The amount of time necessary to perform this measurement with reasonable quality depends strongly on the missing mass resolution of the spectrometers. One possible means of further improving the resolution would be to connect the spectrometers directly to the scattering chamber via vacuum tubes. This modification would eliminate the detrimental effects of multiple scattering in the windows of the scattering chamber and spectrometer. Since we do not plan to move the spectrometers during our experiment, these tubes could remain in place for the entire allotted beam time.

The background could be almost completely eliminated if one of the decay products of the ϕ could be detected in coincidence with the scattered electron and proton. To achieve a three-arm experiment, the K_L^0 from the $\phi \rightarrow K_L^0 K_S^0$ decay could be measured in a calorimeter setup such as the NPS with a backing hadronic calorimeter or tail catcher. Another option would be to utilize, e.g., the HKS to detect one of the charged kaons from the $\phi \rightarrow K^+ K^-$ decay. The SBS, with both tracking and hadronic calorimetry, could in principle measure both the charged and neutral decay modes, thereby

Source	Bin 1	Bin 2	Bin 3	Bin 4	High- $ t $ Bin 1	High- $ t $ Bin 2
Signal Extraction	8.8%	6.5%	8.3%	6.8%	6.7%	10.1%
Rad. Corr. & Fitting Losses	4.0%	4.1%	4.8%	3.1%	3.7%	3.4%
Background Modelling	4.0%	4.0%	4.0%	4.0%	4.0%	4.0%
Tracking Efficiency	0.5%	0.5%	0.5%	0.5%	2.5%	2.5%
Other Systematics	3.0%	3.0%	3.0%	3.0%	3.0%	3.0%
Total Point-to-point	10.9%	9.1%	10.8%	9.0%	9.5%	12.0%

Table 4: Projected point-to-point uncertainties on $d\sigma/d|t|$. The first four columns all refer to the projected uncertainties for the low- $|t|$ setting, i.e., bin 1 refers to the lowest bin in $|t|$. The total uncertainty is calculated as the sum in quadrature of the individual uncertainties given in the table.

increasing the acceptance. In any of these cases, the acceptance for the decay particle would likely need to be better than 10% to collect sufficient statistics for a measurement of similar precision to the two-arm case.

4 Summary

Our projected results on $d\sigma/d|t|$ are shown in Fig. 7. The resolution on $D_s(0)$ is below the preferred value of 0.1⁴, as can be seen by comparing the $D_s(0) = 0.1$ and $D_s(0) = -0.1$ curves to the projected data that lie on the $D_s(0) = 0$ curve. The precision of the measurement of $d\sigma/d|t|$ would enable an extraction of $D_s(0)$ with smaller uncertainty than the most precise existing lattice results.

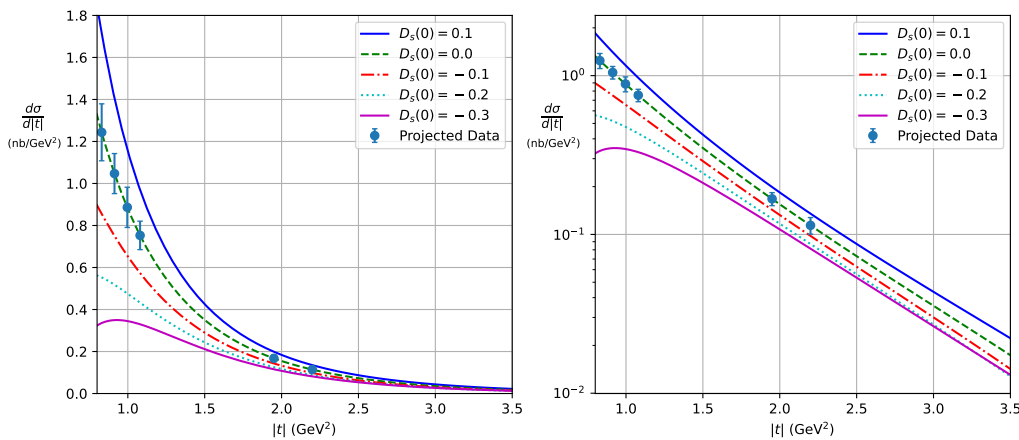


Figure 7: Projected results on $d\sigma/d|t|$ in linear-scale (left panel) and log-scale (right panel) for 297 ab^{-1} (16.5 days at 75 μA) at the low- $|t|$ setting and 207 ab^{-1} (11.5 days at 75 μA) at the high- $|t|$ setting. The projected data points are fixed to the $D_s(0) = 0$ curve. The uncertainties are those listed in Table 4.

To achieve these results, we request 30 days of unpolarized electron beam at 10.6 GeV with a current of 75 μA on the standard Hall C 10 cm LH_2 target. We will use 16.5 of these days for the low- $|t|$ setting, with the HMS central momentum set to 1.1 GeV. For the high- $|t|$ setting with the HMS central momentum set to 1.8 GeV, we will use 11.5 days. We allocate two days for calibration runs and commissioning, bringing the total request to 30 days.

⁴Assuming the dominance of strangeness, as mentioned in Sec. 2.

5 Comparison to Other Experiments and Proposals

The CLAS experiment performed two measurements of exclusive ϕ electroproduction [19, 29] during the 6 GeV era (E-93-022, E-99-105), with beam energies of 4.2 GeV and 5.754 GeV. In both cases, the cross sections were measured as a function of $t' = |t - t_{min.}|$ and Q^2 . The range in Q^2 of the measurement at 4.2 GeV was 0.7 to 2.2 GeV². The measurement at 5.7 GeV extended the kinematic range to $1.4 < Q^2 < 3.8$ GeV². The 5.7 GeV measurement additionally presents the cross section $d\sigma/d|t|$, which is the necessary quantity for extraction of $D_s(0)$. However, as previously mentioned, the authors of the theory prediction were unable to use these results to extract $D_s(0)$, as the measured differential cross section $d\sigma/d|t|$ was integrated over the whole kinematic phase space of the measurement, i.e., $1.4 \leq Q^2 \leq 3.8$ GeV² and $2.10 \leq W \leq 2.90$ GeV. The CLAS $d\sigma/d|t|$ is thus dominated by events at lower Q^2 and, due to the rise of the cross section away from threshold, higher W .

The most similar existing 12 GeV proposal to ours was submitted to PAC 39 under the title “Exclusive Phi Meson Electroproduction with CLAS12” (PR12-12-007) [20]. One of the primary goals of this proposal is to measure the $|t|$ -slope at low $|t|$ for extraction of the high- x gluon GPD. The goal of our study is complementary but different. For the study of $D_s(0)$ as discussed in Sec. 2, the $|t|$ -distribution at low $|t|$ should be measured near-threshold in as small of a window in Q^2 and W as possible. This requirement is uniquely befitting a high luminosity spectrometer setup, where high event statistics can be collected in narrow regions of phase space. An L/T separation of the exclusive ϕ cross section is foreseen in the CLAS12 proposal, but such a procedure is not explicitly necessary for studying $D_s(0)$. The CLAS12 analysis will include measurement of the full final state, including the decay products of the ϕ . Given that our measurement and the CLAS12 measurement will employ independent detectors and analysis techniques, the two will effectively corroborate and enhance the validity of each other’s results.

The CLAS12 ALERT run group has proposed measurements of exclusive ϕ electroproduction on helium-4 and deuterium targets (E12-17-012C) [43]. The comparison of the ϕ electroproduction cross section between proton and nuclear targets is clearly interesting for a multitude of reasons, not the least of which is the fact that helium-4, as the simplest spin 0 system, has non-zero contributions from only the A and D GFFs. While a comparison between proton and nuclear targets directly within CLAS12 is certainly possible, the data we propose to collect will provide an additional proton target reference dataset for the ALERT ϕ program.

The E12-23-004 experiment entitled “A Search for a Nonzero Strange Form Factor of the Proton at 2.5 (GeV/c)²” [44] seeks to measure the strange form factor of the proton via parity-violating elastic scattering. A better knowledge of the contribution of strangeness to the electromagnetic structure of the proton would enhance the interpretation of our proposed results, and we think that this study and ours will together fit nicely into the larger JLab program of studying strangeness in the proton.

An LOI for a measurement of ϕ electroproduction in Hall A utilizing the HRS and SBS was submitted to PAC 35 (LOI-10-002). In this case, the physics goals were similar to those of the two CLAS12 proposals mentioned above; however, a full proposal was not submitted.

6 Other Measurement Opportunities

The $H(e, e'p)$ reaction has the experimental benefit of being “blind” to the decay channels of the additional final state particle or particles. Thus, any particle exclusively produced in this reaction can be measured in the missing mass spectrum. This reaction can be particularly useful for studying the production of particles with more experimentally challenging decay channels. While our primary physics focus is the ϕ , the large momentum acceptance of the SHMS means that our proposed settings also have acceptance for missing masses from roughly 0 to 1.5 GeV, as shown in Fig. 8. We briefly describe here some of the extra measurements that could be made using this data with no additional runtime or changes to the experimental setup.

6.1 Measurement of Non- ϕ Exclusive Meson Final States

Our proposed dataset will provide a large volume of “general-purpose” $H(e, e'p)$ data for the study of exclusive meson production at relatively low values of $|t|$.

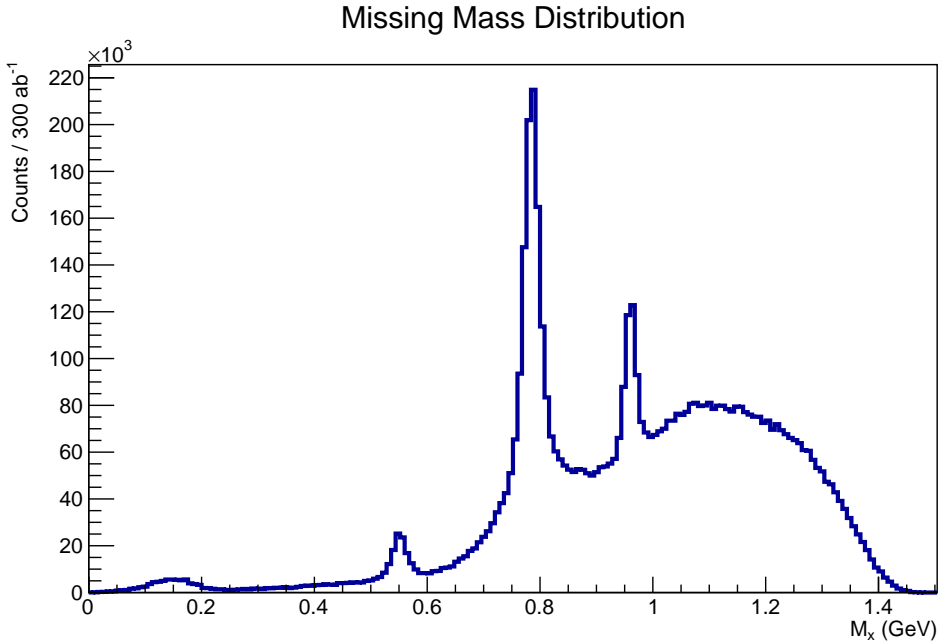


Figure 8: Reconstructed missing mass (M_X) spectra of 297 ab^{-1} of events at our low- $|t|$ setting as simulated by PYTHIA. The peaks corresponding to the π^0 , η , ρ , ω , and η' are all visible. The bin width is 8 MeV. Since this event sample was used for estimating the background to the ϕ , events containing a ϕ have been removed.

The authors of [45] used near-threshold photoproduction data of ω and ϕ to extract the proton mass radius and reached similar results to the mass radius determined using J/ψ data. Our data can serve as a complementary cross check of this result. Additionally, since ratios of exclusive vector mesons can be predicted by GPD models [46], studying the ratios of the ω , ρ , and ϕ production cross sections could serve as a control measurement to better understand both the applicability of GPD models in the near-threshold kinematic region and the interplay of the quark and gluon contributions.

With the data collected by this proposed experiment, the first ever measurement of η' electroproduction could be performed. There was a proposal made to PAC16 (PR-99-109) to perform a measurement of η' electroproduction with CLAS; however, the results were never published. The η' is unique due to its position as a near-flavor-SU(3)-singlet amongst the pseudoscalar mesons and to its unexpectedly large mass, which is generated by the QCD chiral anomaly [47]. PYTHIA6 and LEPTO disagree significantly with both each other and the GPD prediction of Ref. [40] on the magnitude of the η' cross section, and measuring it would provide an anchor point for various future studies, some of which we describe briefly below:

- The CLAS collaboration studied electroproduction of the pseudoscalar mesons η [48] and π^0 [49] at $W > 2 \text{ GeV}$ to access the chiral-odd transversity GPDs. There is also a proposal (E12-06-108) to perform similar measurements with CLAS12. The different quark flavors of the π^0 and η enabled study of the flavor dependence of these GPDs. The assumption has been that strangeness of the η plays no role. Future measurements of hard exclusive production of η' and η , which differ in their strange quark content, can test this assumption. The authors of Ref. [40] computed the total η' cross section, as well as the relative longitudinal and transverse cross sections, using a GPD model. We do not propose to perform an L/T separation of the η' cross section, but the η' cross section is predicted to be dominated by the longitudinal component at low- $|t|$ [40], thus even the total cross section can provide some sensitivity to the GPDs. A measurement of the size and $|t|$ -distribution of the η' cross section could furthermore inform future dedicated measurements targeting the quark-flavor-dependent transversity GPDs.
- The gluon content of the η and η' has long been an active field of study, motivated by the possibility of mixing with glueball states [50–55]. The authors of Ref. [56] proposed electroproduction of

η and η' mesons as a probe of their two-gluon Fock components. These states are also accessible to lattice computations [57–59].

- It is predicted that dense systems such as heavy nuclei or the quark-gluon plasma can facilitate partial restoration of chiral symmetry [60–63], causing the mass of the η' to shift toward smaller values. A similar effect has been proposed to occur within heavy nuclei. Comparing production of η' on proton and nuclear targets would also be interesting from the perspective of color transparency, as was studied in photoproduction in Ref. [64]. A measurement of the magnitude of the η' electroproduction cross section on a proton target could inform further studies in this direction.
- The photoproduction of η' mesons has also been studied extensively in the context of baryonic resonances [65–70], where it serves as an “isospin filter,” allowing for cleaner interpretation of the resonance properties. Recently, the CBELSA/TAPS collaboration provided strong evidence in favor of a resonance at 1895 MeV [66] in the $p\eta'$ channel, which, amongst other known and proposed $p\eta'$ resonances [71], lies well within our proposed kinematic acceptance. The Q^2 dependence of the resonance cross sections is an active field of study [72–74], and electroproduction could provide complementary information to the standard photoproduction process.

7 Acknowledgements

We would like to thank Y. Hatta for providing the theory calculation and for valuable discussion and comments. We also thank L. DeWitt for editing this manuscript.

8 Appendix

8.1 Cross Section Parameterization

We utilize in the above LOI the ϕ electroproduction parameterization from Ref. [20]. This parameterization was fit to the existing data on σ_T, σ_L , and $R = \frac{\sigma_L}{\sigma_T}$ from Cornell, H1, ZEUS, HERMES, NMC, and CLAS. The functional form of the transverse cross section is given as:

$$\sigma_T(W, Q^2) = \frac{c_T(W)}{(1 + Q^2/m_\phi^2)^{\nu_T}}, \quad (6)$$

where ν_T is 3.0 and

$$c_T(W) = \alpha_1 \left(1 - \frac{W_{\text{Th.}}^2}{W^2}\right)^{\alpha_2} \left(\frac{W}{\text{GeV}}\right)^{\alpha_3} \quad (7)$$

in units of nanobarns. $W_{\text{Th.}} = 1.96$ GeV, $\alpha_1 = 400$, $\alpha_2 = 1.0$, and $\alpha_3 = 0.32$. The longitudinal cross section is given as

$$\sigma_L(W, Q^2) = R(W, Q^2)\sigma_T(W, Q^2), \quad (8)$$

where

$$R(W, Q^2) = \frac{c_R}{m_\phi^2} \quad (9)$$

and $c_R = 0.4$. The authors additionally provide two models for the $|t|$ dependence of the cross section, an exponential and a dipole. We provide only the dipole model that we used in our LOI here for compactness. The cross section differential in $|t|$ is given by

$$\frac{d\sigma_{L,T}}{d|t|} = \frac{\sigma_{L,T}F(|t|)}{F_{\text{Int.}}}, \quad (10)$$

where

$$F(|t|) = \frac{m_g^8}{(m_g^2 - t)^4} \quad (11)$$

and

$$F_{\text{Int.}} = \frac{m_g^8}{3(m_g^2 - t_{\text{min.}})^3}. \quad (12)$$

The mass m_g is chosen to be 1 GeV.

References

- [1] Yoshitaka Hatta and Mark Strikman. ϕ -meson lepto-production near threshold and the strangeness D -term. *Phys. Lett. B*, 817:136295, 2021.
- [2] V. D. Burkert, L. Elouadrhiri, and F. X. Girod. The mechanical radius of the proton. 10 2023.
- [3] V. D. Burkert, L. Elouadrhiri, and F. X. Girod. The pressure distribution inside the proton. *Nature*, 557(7705):396–399, 2018.
- [4] V. D. Burkert, L. Elouadrhiri, and F. X. Girod. Determination of shear forces inside the proton. 4 2021.
- [5] V. D. Burkert, L. Elouadrhiri, F. X. Girod, C. Lorcé, P. Schweitzer, and P. E. Shanahan. Colloquium: Gravitational form factors of the proton. *Rev. Mod. Phys.*, 95(4):041002, 2023.
- [6] Maxim V. Polyakov and Peter Schweitzer. Forces inside hadrons: pressure, surface tension, mechanical radius, and all that. *Int. J. Mod. Phys. A*, 33(26):1830025, 2018.
- [7] B. Duran et al. Determining the gluonic gravitational form factors of the proton. *Nature*, 615(7954):813–816, 2023.
- [8] Krešimir Kumerički. Measurability of pressure inside the proton. *Nature*, 570(7759):E1–E2, 2019.
- [9] K. Goetze, Maxim V. Polyakov, and M. Vanderhaeghen. Hard exclusive reactions and the structure of hadrons. *Prog. Part. Nucl. Phys.*, 47:401–515, 2001.
- [10] Daniel C. Hackett, Dimitra A. Pefkou, and Phiala E. Shanahan. Gravitational form factors of the proton from lattice QCD. 10 2023.
- [11] Ho-Yeon Won, Hyun-Chul Kim, and June-Young Kim. Role of strange quarks in the D -term and cosmological constant term of the proton. *Phys. Rev. D*, 108(9):094018, 2023.
- [12] Ho-Yeon Won, Hyun-Chul Kim, and June-Young Kim. Mechanical structure of the nucleon and the baryon octet: Twist-2 case. 10 2023.
- [13] B. Dey, C. A. Meyer, M. Bellis, and M Williams. Data analysis techniques, differential cross sections, and spin density matrix elements for the reaction $\gamma p \rightarrow \phi p$. *Phys. Rev. C*, 89(5):055208, 2014. [Addendum: *Phys.Rev.C* 90, 019901 (2014)].
- [14] K. Mizutani et al. ϕ photoproduction on the proton at $E_\gamma = 1.5 - 2.9$ GeV. *Phys. Rev. C*, 96(6):062201, 2017.
- [15] Renaud Boussarie and Yoshitaka Hatta. QCD analysis of near-threshold quarkonium lepton production at large photon virtualities. *Phys. Rev. D*, 101(11):114004, 2020.
- [16] Philipp Hagler, John W. Negele, Dru Bryant Renner, W. Schroers, T. Lippert, and K. Schilling. Moments of nucleon generalized parton distributions in lattice QCD. *Phys. Rev. D*, 68:034505, 2003.
- [17] Xuan-Bo Tong, Jian-Ping Ma, and Feng Yuan. Gluon gravitational form factors at large momentum transfer. *Phys. Lett. B*, 823:136751, 2021.
- [18] Kazuhiro Tanaka. Operator relations for gravitational form factors of a spin-0 hadron. *Phys. Rev. D*, 98(3):034009, 2018.
- [19] J. P. Santoro et al. Electroproduction of $\phi(1020)$ mesons at $1.4 < Q^{*2} < 3.8$ GeV^{**2} measured with the CLAS spectrometer. *Phys. Rev. C*, 78:025210, 2008.
- [20] H. Avakian et al. Exclusive ϕ meson electroproduction with clas12. https://www.jlab.org/exp_prog/proposals/12/PR12-12-007.pdf. Accessed: 2024-03-13.
- [21] Sang-Ho Kim and Seung-il Nam. Investigation of electroproduction of ϕ mesons off protons. *Phys. Rev. C*, 101(6):065201, 2020.

- [22] F. Cano and J. M. Laget. Compton scattering, vector meson photoproduction and the partonic structure of the nucleon. *Phys. Rev. D*, 65:074022, 2002.
- [23] S. V. Goloskokov and P. Kroll. The Longitudinal cross-section of vector meson electroproduction. *Eur. Phys. J. C*, 50:829–842, 2007.
- [24] S. V. Goloskokov and P. Kroll. Vector meson electroproduction at small Bjorken-x and generalized parton distributions. *Eur. Phys. J. C*, 42:281–301, 2005.
- [25] S. V. Goloskokov and P. Kroll. The Role of the quark and gluon GPDs in hard vector-meson electroproduction. *Eur. Phys. J. C*, 53:367–384, 2008.
- [26] John C. Collins, Leonid Frankfurt, and Mark Strikman. Factorization for hard exclusive electroproduction of mesons in QCD. *Phys. Rev. D*, 56:2982–3006, 1997.
- [27] S. V. Goloskokov. Generalized Parton Distributions in light meson production. *Nucl. Phys. B Proc. Suppl.*, 219-220:185–192, 2011.
- [28] Kiminad A. Mamo and Ismail Zahed. Quark and gluon GPDs at finite skewness from strings in holographic QCD: Evolved and compared with experiment. *Phys. Rev. D*, 108(8):086026, 2023.
- [29] K. Lukashin et al. Exclusive electroproduction of phi mesons at 4.2-GeV. *Phys. Rev. C*, 64:059901, 2001.
- [30] S. Joosten. lager. https://eicweb.phy.anl.gov/monte_carlo/lager. Accessed: 2024-03-31.
- [31] S. Chekanov et al. Exclusive electroproduction of phi mesons at HERA. *Nucl. Phys. B*, 718:3–31, 2005.
- [32] F. D. Aaron et al. Diffractive Electroproduction of rho and phi Mesons at HERA. *JHEP*, 05:032, 2010.
- [33] Roger L. Dixon, R. Galik, D. Larson, A. Silverman, M. Herzlinger, Stephen D. Holmes, F. M. Pipkin, S. Raither, and R. L. Wagner. Spectrometer study of ϕ meson electroproduction. *Phys. Rev. D*, 19:3185, 1979.
- [34] A. Borissov. Proceedings of meson 2000 workshop. In *Proceedings of Meson 2000 Workshop*, pages 19–23, Cracow, Poland, May 2000. DESY.
- [35] Simc, the hall c monte carlo. https://hallcweb.jlab.org/wiki/index.php/SIMC_Monte_Carlo. Accessed: 3-31-24.
- [36] Ruonan Li. *Measurement of the Generalized Polarizabilities of the Proton in Virtual Compton Scattering*. Ph.d. thesis, Temple University, 2022.
- [37] H. Atac et al. Measurement of the N to Δ Transition Form Factors at Low Four Momentum Transfers. https://www.jlab.org/exp_prog/proposals/22/PR12-22-001.pdf. Accessed: 2024-03-13.
- [38] W. B. Li et al. Unique Access to u -Channel Physics: Exclusive Backward-Angle Omega Meson Electroproduction. *Phys. Rev. Lett.*, 123(18):182501, 2019.
- [39] Wenliang Li. *Exclusive Backward-Angle Omega Meson Electroproduction*. PhD thesis, Regina U., 10 2017.
- [40] S. V. Goloskokov and P. Kroll. Transversity in hard exclusive electroproduction of pseudoscalar mesons. *Eur. Phys. J. A*, 47:112, 2011.
- [41] I. Akushevich, H. Bottcher, and D. Ryckbosch. RADGEN 1.0: Monte Carlo generator for radiative events in DIS on polarized and unpolarized targets. In *Workshop on Monte Carlo Generators for HERA Physics (Plenary Starting Meeting)*, pages 554–565, 4 1998.
- [42] A. Gramolin. ESEPP: Event generator of single-electron processes, 2021. Accessed: 2024-04-28.

- [43] Whitney Armstrong et al. Partonic Structure of Light Nuclei. 8 2017.
- [44] B. Wojtsekhowski et al. A search for a nonzero strange form factor of the proton at 2.5 (GeV/c)². <https://misportal.jlab.org/pacProposals/proposals/1862/attachments/174136/Proposal.pdf>. Accessed: 2024-03-13.
- [45] Rong Wang, Wei Kou, Ya-Ping Xie, and Xurong Chen. Extraction of the proton mass radius from the vector meson photoproductions near thresholds. *Phys. Rev. D*, 103(9):L091501, 2021.
- [46] M. Diehl. Generalized parton distributions. *Phys. Rept.*, 388:41–277, 2003.
- [47] Gerard 't Hooft. Symmetry Breaking Through Bell-Jackiw Anomalies. *Phys. Rev. Lett.*, 37:8–11, 1976.
- [48] I. Bedlinskiy et al. Exclusive η electroproduction at $W > 2$ GeV with CLAS and transversity generalized parton distributions. *Phys. Rev. C*, 95(3):035202, 2017.
- [49] I. Bedlinskiy et al. Exclusive π^0 electroproduction at $W > 2$ GeV with CLAS. *Phys. Rev. C*, 90(2):025205, 2014. [Addendum: *Phys.Rev.C* 90, 039901 (2014)].
- [50] D. Robson. A Basic Guide for the Glueball Spotter. *Nucl. Phys. B*, 130:328–348, 1977.
- [51] G. M. Shore and G. Veneziano. Renormalization group aspects of eta-prime \rightarrow gamma gamma. *Nucl. Phys. B*, 381:3–22, 1992.
- [52] Patricia Ball, J. M. Frere, and M. Tytgat. Phenomenological evidence for the gluon content of eta and eta-prime. *Phys. Lett. B*, 365:367–376, 1996.
- [53] Steven D. Bass. Anomalous glue, eta and eta-prime mesons. *Acta Phys. Polon. Supp.*, 2:11–22, 2009.
- [54] Rafel Escribano and Jordi Nadal. On the gluon content of the eta and eta-prime mesons. *JHEP*, 05:006, 2007.
- [55] Wolfgang Ochs. The Status of Glueballs. *J. Phys. G*, 40:043001, 2013.
- [56] Peter Kroll and Kornelija Passek-Kumericki. The Two gluon components of the eta and eta-prime mesons to leading twist accuracy. *Phys. Rev. D*, 67:054017, 2003.
- [57] Eric B. Gregory, Alan C. Irving, Christopher M. Richards, and Craig McNeile. A study of the eta and eta' mesons with improved staggered fermions. *Phys. Rev. D*, 86:014504, 2012.
- [58] H. Fukaya, S. Aoki, G. Cossu, S. Hashimoto, T. Kaneko, and J. Noaki. η' meson mass from topological charge density correlator in QCD. *Phys. Rev. D*, 92(11):111501, 2015.
- [59] Jakob Fabian Simeth. *Properties of the η and η' mesons from lattice QCD*. PhD thesis, Regensburg U., 2022.
- [60] Heinz Pagels. Departures from Chiral Symmetry: A Review. *Phys. Rept.*, 16:219, 1975.
- [61] Edward V. Shuryak. Which chiral symmetry is restored in hot QCD? *Comments Nucl. Part. Phys.*, 21(4):235–248, 1994.
- [62] W. Cassing and E. L. Bratkovskaya. Hadronic and electromagnetic probes of hot and dense nuclear matter. *Phys. Rept.*, 308:65–233, 1999.
- [63] Hideko Nagahiro, Makoto Takizawa, and Satoru Hirenzaki. eta- and eta-prime-mesic nuclei and U(A)(1) anomaly at finite density. *Phys. Rev. C*, 74:045203, 2006.
- [64] M. Nanova et al. Transparency ratio in $\gamma A \rightarrow \eta' A'$ and the in-medium η' width. *Phys. Lett. B*, 710:600–606, 2012.
- [65] V. Crede et al. Photoproduction of eta and eta-prime mesons off protons. *Phys. Rev. C*, 80:055202, 2009.

- [66] F. Afzal et al. Observation of the $p\eta'$ Cusp in the New Precise Beam Asymmetry Σ Data for $\gamma p \rightarrow p\eta$. *Phys. Rev. Lett.*, 125(15):152002, 2020.
- [67] V. L. Kashevarov et al. Study of η and η' Photoproduction at MAMI. *Phys. Rev. Lett.*, 118(21):212001, 2017.
- [68] A. V. Anisovich, V. Burkert, M. Dugger, E. Klempt, V. A. Nikonov, B. G. Ritchie, A. V. Sarantsev, and U. Thoma. Proton- η' interactions at threshold. *Phys. Lett. B*, 785:626–630, 2018.
- [69] L. Tiator, M. Gorchtein, V. L. Kashevarov, K. Nikonov, M. Ostrick, M. Hadžimehmedović, R. Omerović, H. Osmanović, J. Stahov, and A. Švarc. Eta and Etaprime Photoproduction on the Nucleon with the Isobar Model EtaMAID2018. *Eur. Phys. J. A*, 54(12):210, 2018.
- [70] M. Dugger et al. η' photoproduction on the proton for photon energies from 1.527-GeV to 2.227-GeV. *Phys. Rev. Lett.*, 96:062001, 2006. [Erratum: *Phys.Rev.Lett.* 96, 169905 (2006)].
- [71] A. V. Anisovich, V. Burkert, P. M. Collins, M. Dugger, E. Klempt, V. A. Nikonov, B. G. Ritchie, A. V. Sarantsev, and U. Thoma. $N^* \rightarrow N\eta'$ decays from photoproduction of η' -mesons off protons. *Phys. Lett. B*, 772:247–252, 2017.
- [72] I. G. Aznauryan and V. D. Burkert. Electroexcitation of nucleon resonances. *Prog. Part. Nucl. Phys.*, 67:1–54, 2012.
- [73] V. I. Mokeev, P. Achenbach, V. D. Burkert, D. S. Carman, R. W. Gothe, A. N. Hiller Blin, E. L. Isupov, K. Joo, K. Neupane, and A. Trivedi. First Results on Nucleon Resonance Electroexcitation Amplitudes from $ep \rightarrow e'\pi^+\pi^-p'$ Cross Sections at $W = 1.4-1.7$ GeV and $Q^2 = 2.0-5.0$ GeV². *Phys. Rev. C*, 108(2):025204, 2023.
- [74] Victor I. Mokeev and Daniel S. Carman. Photo- and Electrocouplings of Nucleon Resonances. *Few Body Syst.*, 63(3):59, 2022.